RESPONSE TO ANONYMOUS REFEREE #1

"Influence of model spatial resolution on Sargassum beaching predictions along the Mexican Caribbean coast" by de Santos Medina et al.

Review, Referee #1:

This manuscript investigates the influence of ocean model horizontal resolution (5 km versus 1 km) on short-term predictions of Sargassum transport and beaching in the Mexican Caribbean using ROMS, OpenDrift, and FTLE diagnostics. The study addresses a practically relevant question for operational forecasting, and the conclusion that 5-km simulations perform comparably to 1-km simulations except during extreme events and in regions of complex coastal geometry is both interesting and useful. The manuscript is generally well organized and the numerical experiments appear carefully conducted. I nevertheless have several comments regarding the physical interpretation of the results.

1. The particle transport model, $u = u_o + \alpha u_w$, where α is a constant windage coefficient calibrated using undrogued GDP drifters, has become common in Sargassum studies. Nevertheless, it remains an empirical parameterization rather than a dynamical transport model. Recent work by Beron-Vera, Olascoaga, Miron, Bonner and collaborators has shown that reduced finite-size particle models can account simultaneously for inertia, buoyancy, wave effects, and air-water interaction without introducing an ad hoc windage coefficient. Even if such models lie beyond the scope of the present study, the limitations of the adopted parameterization should be acknowledged and the underlying assumptions discussed.

2. The manuscript relies extensively on FTLE fields to identify transport pathways, barriers, attracting structures, retention regions, and likely beaching locations. These interpretations should be stated more carefully. FTLE fundamentally measures finite-time stretching rather than attraction or transport. The distinction between FTLE ridges and objective Lagrangian coherent structures (Haller, Beron-Vera) should also be discussed. Furthermore, recent diagnostics developed specifically for finite-size floating material (Beron-Vera, Olascoaga, Miron, Bonner) identify attracting transport pathways directly from the effective dynamics rather than indirectly through deformation diagnostics.

3. The study compares two spatial resolutions while keeping the transport model fixed. Consequently, the conclusions concern the influence of spatial resolution under the adopted transport model rather than the intrinsic predictability of Sargassum transport. This distinction deserves explicit mention in the Conclusions.

4. Throughout the manuscript, differences between the 5-km and 1-km simulations are frequently attributed to submesoscale structures resolved only by the finer grid. Since these structures are not independently diagnosed, this interpretation should either be supported with additional diagnostics or presented more cautiously.

5. The Introduction would benefit from a clearer statement of the main scientific contributions of the paper. Likewise, terminology such as "transport pathways," "attracting structures," "retention," and "barriers" should be used more precisely, as these refer to distinct dynamical concepts.

Overall, I believe the manuscript constitutes a useful contribution to operational Sargassum forecasting. Addressing the comments above would strengthen both the physical interpretation and the connection with the contemporary literature on Lagrangian transport of finite-size floating material.

Reply to Referee #1:

Thank you very much for your review, we are very pleased with your comments. Please find below our answers and the modifications on the manuscript (in red) related to each of your comments. The insertions are referred to the line numbers of the preprint.

Response to Comment #1: We agree that the results of this study are constrained by the transport model employed and by the simplifying assumptions used to represent drifting Sargassum. We also agree that it is important to acknowledge alternative modeling approaches that address the same problem using different physical frameworks. To address your comment, we added the following paragraph in the Discussion section (inserted on line 495) as follows:

"Finally, it is important to note that the transport model adopted in this study is an empirical parameterization of Sargassum advection, in which particles are assumed to behave as passive tracers advected at the ocean surface by the combined effect of ocean currents and winds. This assumption limits the scope of our results, as the optimal windage factor depends on the regional oceanic and atmospheric conditions, the drifter observations used for calibration and validation, and the oceanic and atmospheric forcing fields used to drive the particle advection model (Berline et al., 2020; Johns et al., 2020; Johnson et al., 2020; Lara-Hernandez et al., 2024; Podlejski et al., 2023; Putman et al., 2020; Putman et al., 2018). In addition, this approach provides a simplified representation of Sargassum transport because it neglects the inertial effects of Sargassum rafts, which can influence their vertical motion within the water column as well as their interaction with surface winds and oceanic structures such as mesoscale eddies (Andrade-Canto et al., 2022; Beron-Vera et al., 2015; Beron-Vera and Miron, 2020; Beron-Vera, 2021; Brooks et al., 2019; Miron et al., 2020). Consequently, our findings should be interpreted within the context of the adopted transport model and its parameterization, rather than as a general characterization of Sargassum transport. Assessing whether our conclusions remain valid under alternative modeling frameworks, such as the approach proposed by Beron-Vera and Miron (2020), which explicitly accounts for the inertial effects of Sargassum rafts, remains an important direction for future research."

Accordingly, we added the following references to the References section:

Inserted on line 605: Beron-Vera, F. J.: Nonlinear dynamics of inertial particles in the ocean: from drifters and floats to marine debris and Sargassum, Nonlinear Dyn., 103, 1–26, https://doi.org/10.1007/s11071-020-06053-z, 2021.

Inserted following the previous reference line (605): Beron-Vera, F. J. and Miron, P.: A minimal Maxey-Riley model for the drift of Sargassum rafts, J. Fluid Mech., 904, A8, https://doi.org/10.1017/jfm.2020.666, 2020.

Inserted on line 607: Beron-Vera, F. J., Olascoaga, M. J., Haller, G., Farazmand, M., Triñanes, J., and Wang, Y.: Dissipative inertial transport patterns near coherent Lagrangian eddies in the ocean, Chaos, 25, 087412, https://doi.org/10.1063/1.4928693, 2015.

Inserted on line 703: Miron, P., Olascoaga, M. J., Beron-Vera, F. J., Putman, N. F., Triñanes, J., Lumpkin, R., and Goni, G. J.: Clustering of marine-debris- and Sargassum-like drifters explained by inertial particle dynamics, Geophys. Res. Lett., 47, e2020GL089874, https://doi.org/10.1029/2020GL089874, 2020.

Response to Comment #2: We thank the reviewer for this important clarification. We agree that the original manuscript attributed a stronger dynamical interpretation to the FTLE fields than is warranted by this diagnostic alone. We have therefore substantially revised the description and interpretation of FTLE throughout the Methods, Results, Discussion, and Conclusions. In the revised manuscript, FTLE is explicitly described as a diagnostic of the maximum finite-time stretching experienced by neighboring trajectories under the adopted particle-advection velocity field. We no longer interpret high FTLE values or FTLE ridges themselves as direct measures of particle transport, accumulation, retention, transport barriers, or beaching. Forward- and backward-time FTLE ridges are instead described, where appropriate, as candidate repelling and attracting material structures, respectively. We have also added a discussion distinguishing this commonly used FTLE-ridge interpretation from the variational and geodesic definitions of objective Lagrangian coherent structures and material transport barriers developed by Haller (2011), Haller and Beron-Vera (2012), and reviewed by Haller (2015). Accordingly, transport routes and beaching patterns in the revised manuscript are inferred primarily from the OpenDrift particle trajectories, final particle distributions, stranding percentages, and stranding times. The FTLE fields are used as a complementary diagnostic to characterize and compare the geometry and intensity of finite-time trajectory deformation between the 5-km and 1-km configurations.

We modified section 2.2 Finite-time Lyapunov exponents (FTLE) fields as follows:

To compare the finite-time deformation experienced by neighboring particle trajectories under the 5-km and 1-km configurations, forward- and backward-time finite-time Lyapunov exponent (FTLE) fields were calculated. In this study, FTLE is used as a diagnostic of finite-time trajectory stretching rather than as a direct measure of particle transport, accumulation, retention, or stranding. To construct the FTLE fields, 339 × 229 particles were released on a uniform grid with 2 km spacing covering the entire study area. Particles were advected using surface currents and a windage factor of 2.5%, and a free-slip boundary condition was applied at the coast to ensure continuous FTLE fields.

Forward and backward FTLE fields were computed for each case by seeding particles on the regular grid and advecting them for 10 days using a time step of 300 s. For the forward simulations, particles were initialized on the first day of each case and integrated forward in time for 10 days. Conversely, for the backward simulations, particles were initialized on the last day of each case and integrated backward in time for 10 days.

FTLE quantifies the maximum finite-time stretching of initially neighboring trajectories (Peng et al., 2024). To compute these rates, particles are initially distributed on a uniform grid with positions X_0 at time t_0. The particles are then advected over a time T, and the resulting deformation of fluid parcels is quantified using the Cauchy-Green strain tensor. The FTLE at each point is derived from the largest eigenvalue of this tensor, following the formulation of Haller (2001):

$$\sigma_{t_0}^{T} = \frac{\mathbf{1}}{|\boldsymbol{T}|}\ln(\lambda_{max}) \quad (2)$$

Where σ^{T}_{t0} is the FTLE, λ_{max} is the maximum eigenvalue of the Cauchy-Green strain tensor, and T is the integration interval. Ridges of forward-time FTLE are commonly interpreted as candidate repelling material structures, whereas ridges of backward-time FTLE may indicate candidate attracting material structures (Peng et al., 2024). However, FTLE ridges do not necessarily satisfy the variational or geodesic conditions defining objective Lagrangian coherent structures or material transport barriers (Haller, 2011;

Haller, 2015; Haller and Beron-Vera, 2012). Accordingly, we use FTLE primarily to compare finite-time deformation patterns between model configurations.

Accordingly, we added the following references to the References section (inserted on line 650):

Haller, G.: A variational theory of hyperbolic Lagrangian Coherent Structures, Phys. D, 240, 574–598, https://doi.org/10.1016/j.physd.2010.11.010, 2011.

Haller, G.: Lagrangian Coherent Structures, Annu. Rev. Fluid Mech., 47, 137–162, https://doi.org/10.1146/annurev-fluid-010313-141322, 2015.

Haller, G. and Beron-Vera, F. J.: Geodesic theory of transport barriers in two-dimensional flows, Phys. D, 241, 1680–1702, https://doi.org/10.1016/j.physd.2012.06.012, 2012.

We also applied the following modifications to the section 3.1 FTLE of the Results section:

To compare finite-time deformation patterns between the 5- and 1-km configurations, forward and backward FTLE fields were analysed for each case. In the Mean Circulation case, bands of elevated forward-time FTLE occur along the northern edge of the Cayman/Yucatan Current in both configurations (Fig. 2a, 2b), indicating strong finite-time stretching of neighboring trajectories. The 1-km field exhibits finer and more filamentary deformation patterns than the 5-km field. These elevated-FTLE regions are spatially aligned with the Cayman/Yucatan Current, while the particle simulations show dominant particle advection toward Cozumel. Both configurations also exhibit elevated forward-time FTLE extending from the southeastern part of the domain toward the Islas de la Bahía. In the Gulf of Honduras, FTLE values are generally lower, although numerous filamentary deformation features are present. In the 5-km configuration, an additional band of elevated FTLE extends from the Cayman Current toward Xcalak; this feature is less pronounced in the 1-km configuration.

Backward-time FTLE fields exhibit pronounced ridges around and north of Cozumel in both configurations (Fig. 2c, 2d). Such backward-time FTLE ridges indicate strong backward-time stretching and may be interpreted as candidate attracting material structures, although they do not by themselves demonstrate particle accumulation or retention. The 1-km field contains a curved, eddy-shaped FTLE ridge that is absent or less clearly defined in the 5-km field. Both configurations also exhibit numerous filamentary backward-time FTLE ridges in the Gulf of Honduras and around Banco Chinchorro, indicating spatially complex finite-time deformation in these regions.

In the Tropical Cyclone case, forward-time FTLE fields exhibit a more spatially fragmented deformation pattern in both configurations (Fig. 2e, 2f), with numerous filamentary regions of enhanced stretching. These features are finer and more numerous in the 1-km configuration. In the 5-km field, a high-FTLE filament extends toward Cancun, whereas the corresponding feature is weaker in the 1-km field. A similar difference occurs east of Xcalak.

Backward-time FTLE fields exhibit a dipole-like deformation pattern in both configurations (Fig. 2g, 2h), more clearly defined in the 5-km field. In the 5-km configuration, an elongated backward-time FTLE ridge extends from Cozumel toward the Gulf of Mexico and subsequently westward along the northern Yucatan coast, whereas in the 1-km configuration the corresponding ridge extends northward without the same westward curvature. Additional backward-time FTLE ridges occur near Xcalak, the Islas de la Bahía, the Gulf of Honduras, and Cuba.

In the Large Ro case, forward FTLE fields exhibit high values along the northern edge of the Cayman Current towards Cozumel in both grids (Fig. 2i, 2j). These values are higher in the 5-km grid than in the 1-km grid, and in the 5-km grid the Cayman Current shows numerous filaments and instabilities. South of Cuba, high-value filaments are observed in both grids; these are more pronounced in the 1-km grid, which may indicate circulation around Cuba. In both grids, filaments originate southeast of the Islas de la Bahia and extend towards the Turneffe islands. In the Gulf of Honduras, FTLE values are low in both grids, although numerous filaments are present. In the 5-km grid, some filamentary FTLE features show higher values than in the 1-km configuration and extend toward Banco Chinchorro and northward along the coast.

Backward FTLE fields display high values in both grids (Fig. 2k, 2l) within the Gulf of Honduras, associated with filaments originating from the Islas de la Bahia and reaching the coasts south of Xcalak. High-value filaments also emerge from Banco Chinchorro towards the north in both grids. From Cozumel, high values extend towards the Gulf of Mexico; in the 1-km grid, these filaments reach westward along the northern coast of the Yucatan Peninsula. High FTLE values are also observed in the Yucatan Channel in both grids. South of Cuba, high-value filaments appear in both grids, likely induced by the presence of eddies.

In the Anticyclonic Eddy case, forward FTLE fields in both grids (Fig. 2m, 2n) exhibit maxima along the boundary of the anticyclonic eddy located south of Cuba, indicating enhanced finite-time stretching around the eddy. Elevated FTLE values also occur along the Cayman/Yucatan Current. Independently, particle simulations show substantial particle advection toward Cozumel. Elevated forward-time FTLE is also observed southeast of the Islas de la Bahía, while values in the Gulf of Honduras are generally lower and more filamentary.

Backward FTLE fields reveal high values around and north of Cozumel in both grids (Fig. 2o, 2p). Elevated backward-time FTLE also occurs around and north of Banco Chinchorro, particularly in the 5-km configuration. These patterns indicate differences in finite-time deformation between the configurations.

We made the following modifications to lines 351-353:

"…and 2.04%). The Tropical Cyclone case exhibits the largest resolution-dependent differences in particle stranding among the four cases. The Rossby-number analysis presented in Appendix B shows enhanced small-scale vorticity and broader Rossby-number distributions in the 1-km configuration, consistent with a stronger representation of submesoscale variability. Together with the resolution-dependent differences observed in the particle trajectories and FTLE deformation patterns, these results suggest that the particle predictions are particularly sensitive to finer-scale circulation variability under tropical-cyclone forcing."

We also modified the Discussion section as follows:

Lines 397-444: "The FTLE analysis provided a complementary description of the finite-time deformation experienced by neighboring particle trajectories under the two model configurations. The OpenDrift simulations indicated that the Cayman and Yucatan Currents constitute the dominant particle-advection route through the study area, directing a substantial fraction of particles toward Cozumel. Bands of elevated forward-time FTLE were spatially aligned with these currents, indicating strong finite-time stretching adjacent to the dominant advective flow. Backward-time FTLE ridges occurred around and north of Cozumel, Banco Chinchorro, and within the Gulf of Honduras, indicating regions of enhanced backward-time stretching that may be regarded as candidate attracting material structures. We do not, however, interpret these FTLE features alone as evidence of particle accumulation, retention, transport barriers, or likely landing sites. These quantities were assessed from the OpenDrift particle distributions and stranding diagnostics, while FTLE was used to provide dynamical context for the deformation of neighboring trajectories.

Allende-Arandia et al. (2023) used climatological Lagrangian coherent structures (cLCSs) to characterize persistent transport organization from the tropical Atlantic toward the Caribbean Sea and Gulf of Mexico. Their analysis identified the Yucatan Current as a persistent feature organizing along-current transport while restricting cross-current exchange toward the Mexican coast, with this organization weakened when wind forcing was included. The cLCS framework used in that study differs from the FTLE diagnostic employed here, and we therefore do not interpret our forward-time FTLE ridges as material transport barriers. In the Mean Circulation, Large Ro, and Anticyclonic Eddy cases, elevated forward-time FTLE occurs along the Yucatan Current (Fig. 2a, b, i, j, m, n), indicating strong finite-time stretching in the vicinity of the current. The OpenDrift trajectories independently show dominant along-current advection, consistent with the importance of the Yucatan Current in organizing regional Sargassum transport. Likewise, in many other coastlines with boundary currents, the onshore transport of larvae depends on factors that debilitate or break the predominant alongshore flow (Harrison and Siegel, 2014) as well as on conditions that generate across shore flows such as onshore winds (Caputi et al., 2002) or eddies (Cetina-Heredia et al., 2019; Roughan et al., 2022).

During the Tropical Cyclone case, forward-time FTLE values are generally lower and the high-FTLE regions associated with the Cayman/Yucatan Current are less continuous than in the other cases (Fig. 2e, 2f). This indicates weaker or more spatially fragmented finite-time stretching over the selected 10-day interval, rather than necessarily weaker transport. The OpenDrift simulations independently show larger resolution-dependent differences in particle trajectories and strandings during this case. Thus, the altered FTLE geometry is interpreted as evidence of changes in trajectory deformation, while changes in particle transport are assessed directly from the particle simulations.

The largest differences in particle stranding between the model configurations occur during the Tropical Cyclone case. The Rossby-number analysis in Appendix B indicates enhanced small-scale vorticity and a greater occurrence of large Rossby numbers in the 1-km configuration, consistent with enhanced submesoscale variability. The particle simulations also display greater divergence between resolutions during this case, while the FTLE fields indicate corresponding differences in finite-time deformation. Collectively, these diagnostics suggest that short-term particle predictions become more sensitive to ocean-model resolution when intense atmospheric forcing modifies the small-scale circulation.

The highest particle-landing percentages across the four cases occurred around Cozumel, Banco Chinchorro, the Sian Ka'an Reserve, and northern Cancun (Fig. 4). The FTLE fields exhibit regions of enhanced finite-time deformation around several of these locations, including backward-time FTLE ridges around Banco Chinchorro and north of Cozumel. These spatial correspondences provide complementary information on the deformation experienced by nearby trajectories, whereas the identification of landing hotspots is based directly on the OpenDrift stranding simulations."

Lines 460-469: "In Jouanno et al. (2025), the annual Sargassum biomass was estimated from 2018 to 2023; they reported that the coastline from Xcalak to Puerto Morelos receives approximately 100,000 tons of Sargassum biomass per year, the western Cuban coast receives about 40,000 tons, and the Islas de la

Bahia receives less than 20,000 tons per year. In agreement, our results registered strandings along the coast from Xcalak to Puerto Morelos (Fig. 4), possibly associated with Sargassum transport by the Yucatan Current and its interaction with onshore winds. Our particle simulations also produce strandings along the Cuban coast and the Islas de la Bahía (Fig. 4). Around Cuba, these particle trajectories occur in a region characterized by mesoscale eddying circulation, while the FTLE fields show pronounced deformation around the corresponding eddy boundaries. The FTLE patterns alone do not establish eddy-driven retention or attraction, but their spatial correspondence with the particle trajectories is consistent with an influence of mesoscale circulation on particle redistribution. For the Islas de la Bahía, the simulated trajectories indicate direct transport from particles released south of the core of the Cayman Current."

And we modified the Conclusions section as follows:

Lines 503-509: "The highest stranding percentages were consistently observed around Cozumel, Banco Chinchorro, the Sian Ka'an Reserve, and the northern coast of Cancun, in agreement with previous observational and modelling studies (Chavez et al., 2020; Lara-Hernandez et al., 2024; Jouanno et al., 2025; Uribe-Martinez et al., 2022). Due to their exposure to prevailing currents and the orientation of the coastline, these regions are particularly vulnerable to massive Sargassum landings (Lara-Hernandez et al., 2024; Uribe-Martinez et al., 2022). The particle simulations identify recurrent advective routes associated with the Cayman and Yucatan Currents and show that mesoscale and coastal circulation features influence the spatial distribution of particles and landings. The FTLE fields provide complementary information on finite-time trajectory deformation in these regions."

Response to Comment #3: We agree that the results of this study are constrained by the transport model employed and its associated limitations. Accordingly, we modified the Conclusions section as follows (line 511):

"Our results suggest that for operational and short-term forecasting purposes, using models with a 5 km spatial resolution is sufficient to represent the general distribution and timing of Sargassum strandings in the region. However, in areas with high geomorphological complexity or during extreme events, higher-resolution models (1 km) can provide improvements in spatial accuracy of landings and associated biomass estimates. Additionally, a detailed representation of the coastline is essential in simulations, as it directly influences stranding patterns.

It is important to note that our conclusions are representative of the influence of spatial resolution within the transport model used, including its underlying assumptions and the simplification of representing Sargassum as passive particles transported at the ocean surface. Consequently, our findings should be interpreted within the context of this modelling framework and not as a measure of the intrinsic predictability of Sargassum transport. Rather, they reflect the behaviour of passive tracers in a model calibrated to approximate Sargassum advection using undrogued drifters as a proxy. Ultimately, this study contributes to the development and optimization of more robust forecasting tools that can aid Sargassum collection and mitigation strategies, thereby minimizing its ecological and socioeconomic impacts in the Mexican Caribbean."

Response to Comment #4: We agree that the comparison between the 5-km and 1-km simulations would benefit from a more explicit dynamical diagnosis of the small-scale features represented by the higher-resolution configuration. To address this comment, we have added a new Appendix (Appendix B) presenting daily-mean Rossby-number fields for each of the four study cases, together with probability density functions (PDFs) and associated statistics. The Rossby number was calculated as ($Ro=\zeta/f$), where ζ is the vertical component of the relative vorticity derived from the daily-mean surface currents and (f) is the Coriolis parameter. For each study case, we present Rossby number maps for days 1, 4, 7, and 10 to illustrate the spatial differences between the two model configurations and the finer-scale fronts, filaments, and wake structures represented in the 1-km simulation.

In addition, we calculated independently normalized daily PDFs of the Rossby number and averaged them over each study period. We also report the standard deviation, skewness, 95th and 99th percentiles, and the probability of ($|Ro|>1$) for each model configuration. The 1-km simulation generally exhibits broader Rossby number distributions, stronger positive skewness, larger upper-tail values, and a greater occurrence of ($|Ro|>1$) than the 5-km simulation. These characteristics are consistent with an enhanced representation of submesoscale variability in the higher-resolution configuration, as submesoscale flows are commonly associated with elevated Rossby numbers, strong relative vorticity, fronts and filaments, and positively skewed vorticity distributions. We have therefore used these additional diagnostics to better support the interpretation of the differences between the two simulations.

Therefore, we made the following changes to the manuscript (inserted as Appendix B):

Appendix B

To compare the ocean current fields from the 5-km and 1-km ROMS simulations and assess the representation of submesoscale features in the higher-resolution configuration, we calculated maps of the daily-mean Rossby number ($Ro=\zeta/f$) for each of the study cases. The Rossby number was computed as the ratio of the vertical component of the relative vorticity (ζ) of the surface ocean currents to the Coriolis parameter (*f*). Rossby-number fields were derived from the daily mean surface currents produced by the 5-km and 1-km ROMS configurations. Furthermore, an independently normalized probability density function (PDF) of the Rossby number was calculated for each day, and the daily PDFs were averaged to obtain a mean PDF for each study case and model configuration. The standard deviation (σ), skewness (Sk), 95th percentile (P95), and 99th percentile (P99) were calculated from the pooled Rossby-number values over each study period, while the probability of $|Ro|>1$ was calculated daily and then averaged over the study period.

Submesoscale flows are typically characterized by horizontal scales of approximately 0.1 to 10 km and often manifest as narrow fronts and filaments where the local Rossby number reaches O(1) (Thomas et al., 2008). Additionally, submesoscale flows often exhibit positively skewed distributions of relative vorticity, with the magnitude of the skewness varying with season, depth, and spatial scale or resolution (Buckingham et al., 2016; Shcherbina et al., 2013).

Across all case studies (Fig. B1, B2, B3, B4), enhanced relative vorticity and elevated Rossby numbers are observed in the wakes of the islands, particularly downstream of Banco Chinchorro and Cozumel. These wake structures are more confined to the coastline in the 1-km simulation than in the 5-km configuration. Compared with the 5-km simulation, the 1-km configuration also represents numerous narrow filaments around the Islas de la Bahía. In contrast to the wakes downstream of Banco Chinchorro and Cozumel, these filaments are largely absent or poorly resolved in the 5-km simulation.

Although the large-scale circulation patterns are similar in both simulations, the 1-km configuration represents substantially finer elongated bands and filaments of elevated Rossby number, consistent with submesoscale structures (Thomas et al., 2008). These features are particularly evident around the Islas de la Bahía, the Turneffe Islands, Cozumel, and Banco Chinchorro. During the Tropical Cyclone case (Fig. B2), filamentary structures also develop offshore, extending beyond the immediate coastal environment.

The Rossby-number distributions (Fig. B5) show greater standard deviation in the 1-km configuration than in the 5-km configuration for all study cases (Mean circulation: 0.63 vs. 0.38; Tropical cyclone: 0.36 vs. 0.22; Large Ro: 0.58 vs. 0.38; Anticyclonic eddy: 0.46 vs. 0.30). Skewness is also consistently higher in the 1-km configuration (Mean circulation: 3.07 vs. 0.87; Tropical cyclone: 2.84 vs. 1.33; Large Ro: 2.36 vs. 0.88; Anticyclonic eddy: 3.42 vs. 1.12). The 95th percentile is higher at 1 km for the Mean circulation (0.63 vs. 0.53), Tropical cyclone (0.44 vs. 0.34), and Large Ro (0.70 vs. 0.54) cases, while it is identical for the Anticyclonic eddy case (0.44 in both configurations). The 99th percentile is higher in the 1-km configuration for all cases (Mean circulation: 2.43 vs. 1.47; Tropical cyclone: 1.30 vs. 0.81; Large Ro: 2.10 vs. 1.41; Anticyclonic eddy: 1.69 vs. 1.12). Similarly, the probability of |Ro|>1 is consistently greater at 1 km (Mean circulation: 3.97% vs. 3.20%; Tropical cyclone: 2.23% vs. 0.71%; Large Ro: 4.20% vs. 2.58%; Anticyclonic eddy: 2.65% vs. 1.88%). Overall, the broader distributions, stronger positive skewness, larger upper-tail percentiles, and increased occurrence of |Ro|>1 in the 1-km configuration are consistent with an enhanced representation of submesoscale variability relative to the 5-km simulation.

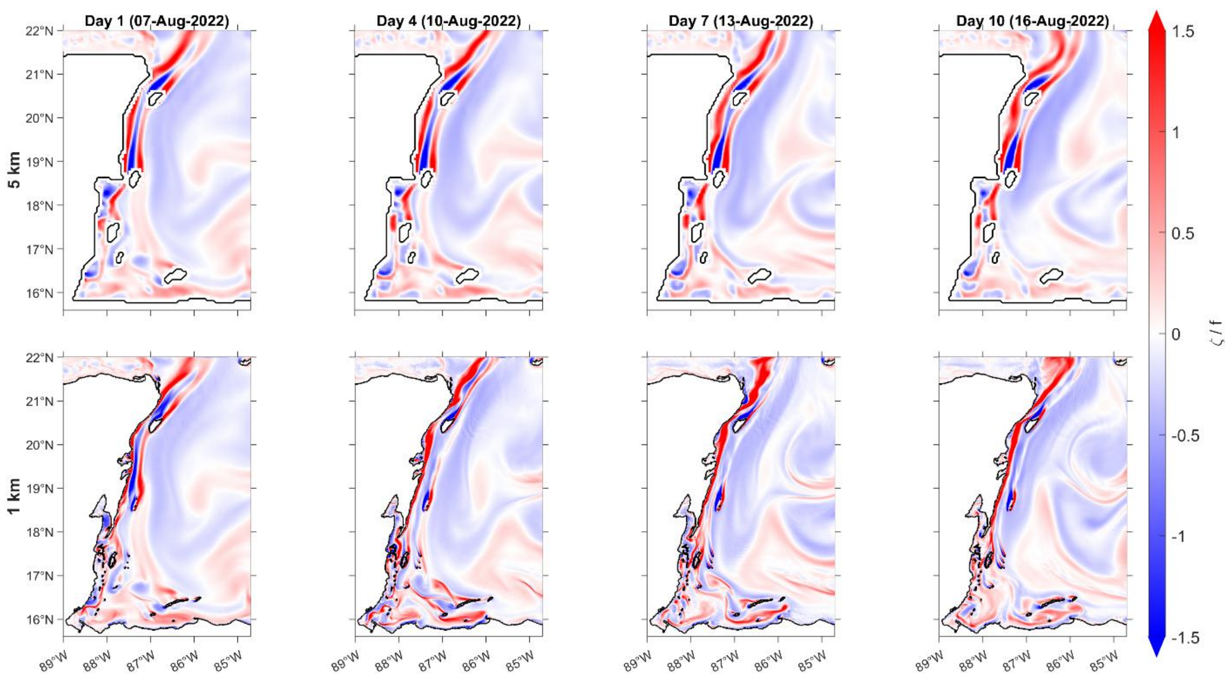

Fig. B1: Daily-mean Rossby number (ζ / f) fields calculated from surface ocean currents simulated with ROMS configured at 5 km (upper panels) and 1 km (lower panels) horizontal resolution. The panels show the daily mean fields for the Mean Circulation (7–17 August 2022) case on simulation days 1, 4, 7, and 10.

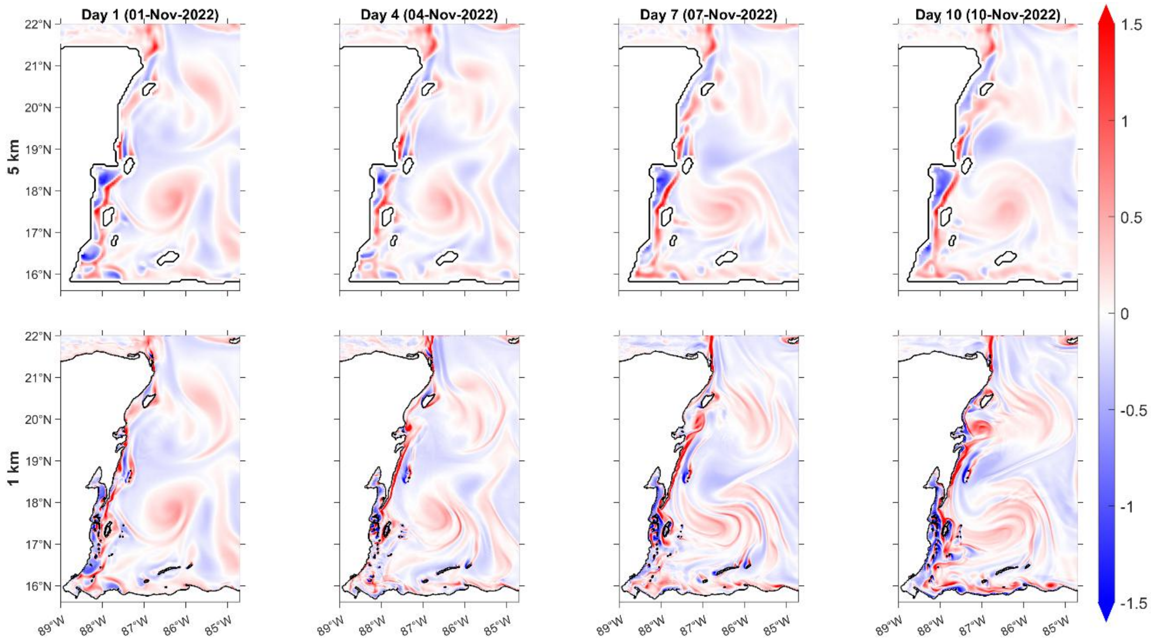

Fig. B2: Daily-mean Rossby number (*ζ / f*) fields calculated from surface ocean currents simulated with ROMS configured at 5 km (upper panels) and 1 km (lower panels) horizontal resolution. The panels show the daily mean fields for the Tropical Cyclone (1–11 November 2022) case on simulation days 1, 4, 7, and 10.

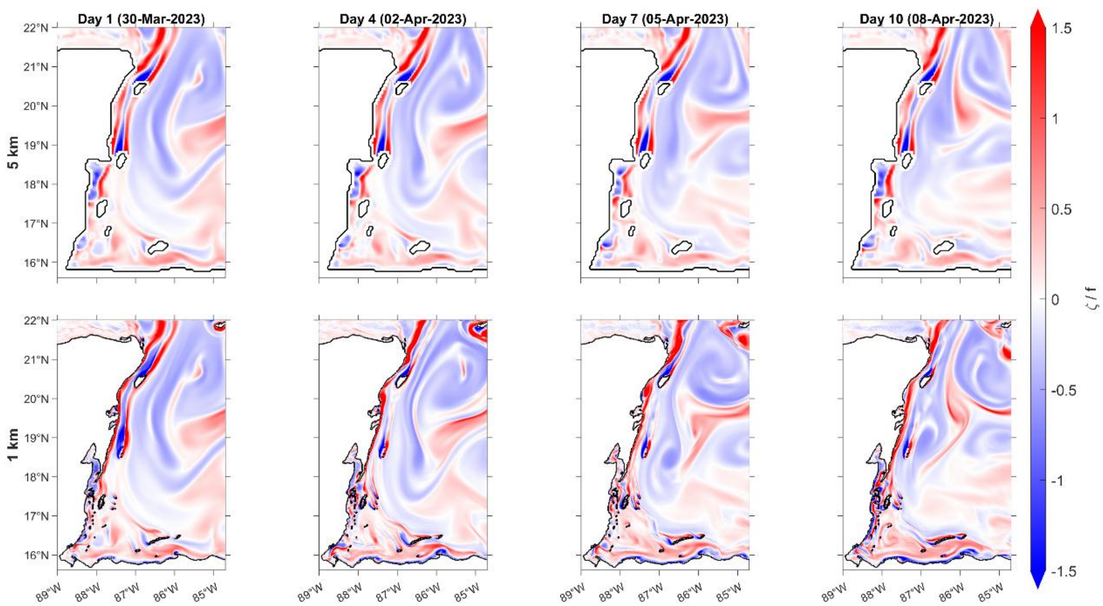

Fig. B3: Daily-mean Rossby number (*ζ / f*) fields calculated from surface ocean currents simulated with ROMS configured at 5 km (upper panels) and 1 km (lower panels) horizontal resolution. The panels show the daily mean fields for the Large Ro (30 March–9 April 2023) case on simulation days 1, 4, 7, and 10.

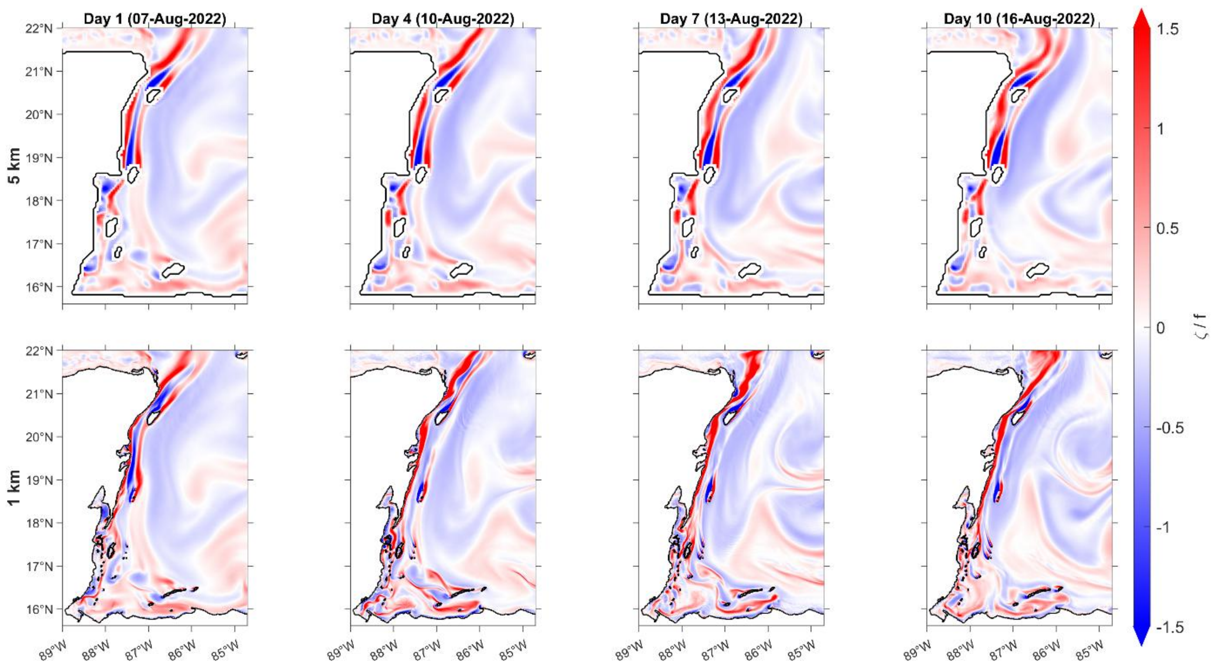

Fig. B4: Daily-mean Rossby number (ζ / f) fields calculated from surface ocean currents simulated with ROMS configured at 5 km (upper panels) and 1 km (lower panels) horizontal resolution. The panels show the daily mean fields for the Anticyclonic Eddy (10–20 June 2023) case on simulation days 1, 4, 7, and 10.

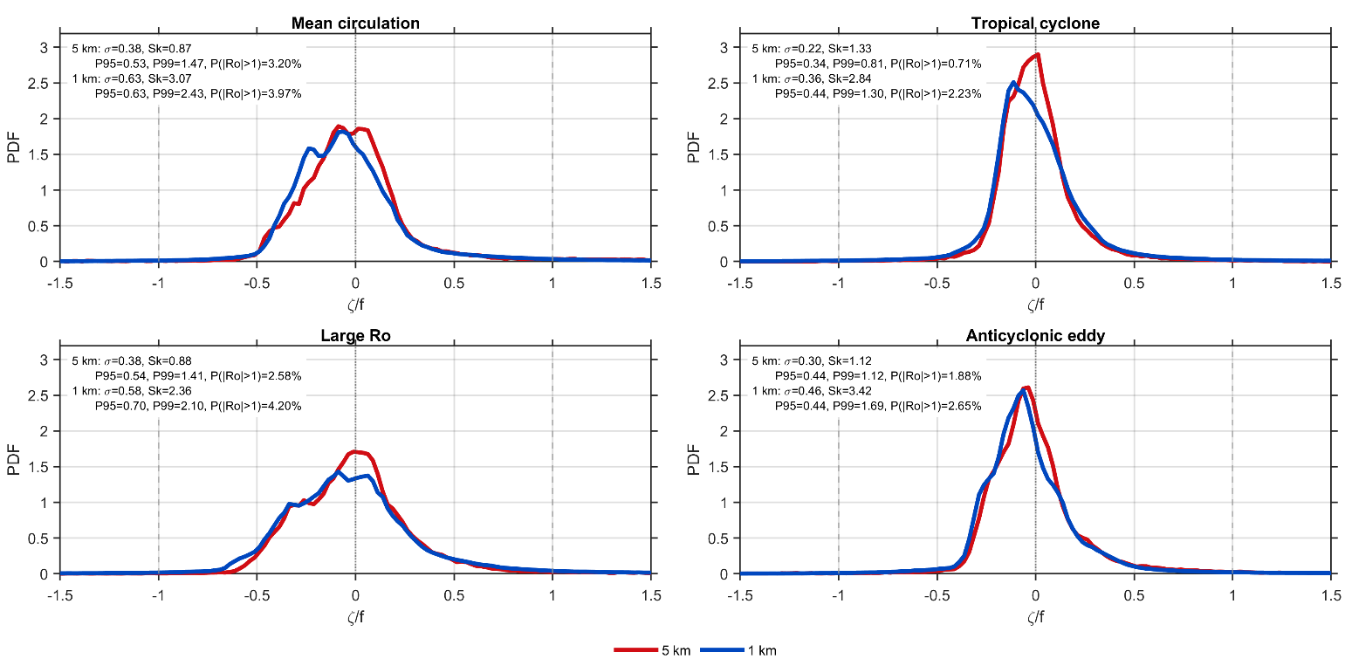

Fig. B5: Mean of the independently normalized daily probability density functions (PDFs) of the Rossby number (Ro= ζ /f), calculated from daily-mean surface ocean current fields from the 5-km (red) and 1-km (blue) ROMS configurations. PDFs are shown for the four study cases: Mean circulation, Tropical

cyclone, Large Ro, and Anticyclonic eddy. Each panel reports the standard deviation (σ), skewness (Sk), 95th percentile (P95), 99th percentile (P99), and probability of |Ro|>1 for each configuration.

Accordingly, we added the following references to the References section:

Inserted on line 616: Buckingham, C. E., Naveira Garabato, A. C., Thompson, A. F., Brannigan, L., Lazar, A., Marshall, D. P., George Nurser, A. J., Damerell, G., Heywood, K. J., and Belcher, S. E.: Seasonality of submesoscale flows in the ocean surface boundary layer, Geophys. Res. Lett., 43, 2118–2126, https://doi.org/10.1002/2016GL068009, 2016.

Inserted on line 755: Shcherbina, A. Y., D'Asaro, E. A., Lee, C. M., Klymak, J. M., Molemaker, M. J., and McWilliams, J. C.: Statistics of vertical vorticity, divergence, and strain in a developed submesoscale turbulence field, Geophys. Res. Lett., 40, 4706–4711, https://doi.org/10.1002/grl.50919, 2013.

Inserted on line 761: Thomas, L. N., Tandon, A., and Mahadevan, A.: Submesoscale processes and dynamics, Ocean Modeling in an Eddying Regime, in: Ocean Modeling in an Eddying Regime, Geophys. Monogr. Ser., edited by: Hecht, M. W. and Hasumi, H., AGU, Washington D. C., United States of America, 17–38, https://doi.org/10.1029/177GM04, 2008.

Response to Comment #5: We agree that the principal scientific contribution of the study should be stated more explicitly and that terminology describing distinct Lagrangian dynamical concepts should be used more precisely. To address the first point, we have substantially revised the final paragraph of the Introduction to clarify the scientific objective and contribution of the study:

Introduction (lines 75-80): "High-resolution ocean models may improve the representation of circulation processes that influence nearshore Sargassum transport, but their greater computational cost may limit their use in operational forecasting systems. Here, we quantify how the horizontal resolution of the ocean circulation model influences 10-day Sargassum transport and stranding predictions in the Mexican Caribbean under four dynamical regimes. By applying the same wind forcing, particle-transport formulation, release strategy, and stranding criterion to ROMS configurations with horizontal resolutions of 5 km and 1 km, we evaluate the sensitivity of predicted particle distributions, trajectories, stranding percentages, landing locations, and stranding times to model spatial resolution. The main contribution of this study is to determine the dynamical conditions and geographic settings in which a 5-km circulation model produces operationally relevant predictions comparable to those of a 1-km configuration, and to identify situations in which the additional spatial detail of the higher-resolution model materially affects predicted Sargassum landings. This comparison provides a quantitative basis for balancing computational cost and spatial resolution in the development of short-term operational forecasting systems."

To address the terminology issue, we have revised the Abstract, Methods, Results, Discussion, and Conclusions to distinguish among transport, deformation, attraction, retention, and material transport barriers. Some of the changes applied were already included in the revisions related to Comment #2. We applied the following modifications:

Abstract (lines 14-17): "Under typical circulation conditions, both resolutions produce comparable large-scale particle-transport patterns and similar regional landing distributions. In contrast, under extreme event conditions (i.e., tropical cyclone), resolution-dependent differences in the small-scale circulation and particle trajectories become larger, leading to substantial shifts in coastal accumulation patterns."

Introduction (lines 49-51): "Mesoscale eddies have been shown to modulate Sargassum accumulation and redistribution across the tropical Atlantic by altering particle residence, aggregation, and downstream transport (Andrade-Canto et al., 2022; Beron-Vera et al., 2022; Brooks et al., 2019; Sosa-Gutierrez et al., 2025)."

Introduction (lines 58-60): "These findings suggest that model resolution can substantially influence simulated particle trajectories and accumulation patterns, with important implications for Sargassum transport and beaching predictions."

Case study description (lines 175-177): "The fourth case (Anticyclonic Eddy; 10–20 June 2023) is defined by the presence of an anticyclonic eddy south of Cuba and was included to investigate how coherent mesoscale circulation features influence particle distributions, dispersion, and downstream transport."

Discussion (lines 391-393): "The results indicate that, despite local differences in stranding patterns, particularly in regions with complex coastal geometry and during extreme events, the dominant particle trajectories, stranding percentages and mean arrival times are broadly consistent between the two resolutions."